

Article

Efficient Control of a Non-Linear System Using a Modified Sliding Mode Control

Saad Jamshed Abbasi, Karam Dad Kallu and Min Cheol Lee *

School of Mechanical Engineering, Pusan National University, Busandaehak-ro 63beon-gil, Jangjeon-dong Geumjeong-gu, Busan 46241, Korea; saadjamshed93@gmail.com (S.J.A.); karamdadkallu@gmail.com (K.D.K.)

* Correspondence: mclee@pusan.ac.kr; Tel.: +82-10-3861-2688

Received: 29 January 2019; Accepted: 18 March 2019; Published: 27 March 2019



Abstract: Trajectory tracking is an essential requirement in robot manipulator movement and localization applications. It is a current research topic of interest, and several researchers have proposed different schemes to achieve the task accurately. This research proposes efficient control of a hydraulic non-linear robot manipulator using a modified sliding mode control, named proportional derivative sliding mode control with sliding perturbation observer (PDSMCSP0), to overcome parameter uncertainties and non-linearity. The proposed new control strategy achieves higher accuracy and better time convergence than the previous one. A positive derivative gain, which has a value less than one, is multiplied with the velocity error term of the sliding surface. The proposed control (PDSMCSP0) also achieves robustness. Results show that by introducing the derivative gain, the chattering from the system has been reduced more than classical sliding mode control (SMC). The reason is that during reaching phase this small gain multiplies with the perturbation and minimizes the effect of perturbation on the system. A smaller value of switching gain K is required as compared to SMC, and the transfer function between sliding surface and perturbation in proportional derivative sliding mode control (PDSMC) has low pass filter characteristics. The proposed PDSMCSP0 has a faster response than previous sliding mode control with sliding perturbation observer (SMCSP0), and the output and sliding surface convergence to the desired value is much quicker than conventional logic. Some other characteristics such as error in the output are small because of more attenuation of the perturbation signal. Simulation and experimental results are presented for a link between the hydraulic robot manipulator and the mass damper system.

Keywords: sliding mode control; proportional and derivative sliding mode control; sliding observer; sliding perturbation observer

1. Introduction

Decommissioning or dismantling nuclear power plants gained attention all over the world after the Fukushima nuclear power plant incident in Japan. Because of the dynamic or hazardous environment of a nuclear power plant it is better to use a robot, whether it is fully autonomous or semi-autonomous. For the dismantling of massive structures, hydraulic operated robot manipulators have been widely used as high-power actuator [1] and should be controlled by tele-operation because of high radioactive environment problem [2–8]. Hydraulic systems are highly non-linear in nature because they have a lot of uncertainties and non-linearity's. Due to the nature of a hydraulic system, it is complicated to control the system with conventional or linear control logic. To overcome this problem, a robust or non-linear control is needed.

In the last few decades, using sliding mode control (SMC) as a kind of non-linear control has gained much attention among researchers because of its robust nature [9–14]. The main idea is to design a desired sliding surface and force the system states to move towards it by using gain switching.

It is used as a robust controller for a system with non-linearity. However, there is a problem with conventional SMC when the system reaches the sliding surface, because it is difficult to remain along the sliding surface due to a high gain switching control system output crossing back and forth around the sliding surface which causes chattering [15–17].

Chattering can be reduced by perturbation compensation where the perturbation consists of the uncertainties of a system, error of the dynamics, and external disturbances. Perturbation measurement or estimation is a challenging task for researchers because measuring external forces using a force sensor is not feasible in all instances, and by using a sensor we cannot estimate system uncertainties, etc. To overcome this problem Olgac et al. proposed using a sliding perturbation observer (SPO) [2]. SPO is the combination of a perturbation observer and a sliding observer (SO) [3]. SPO used partial state feedback from the non-linear system to estimate other variables in the high-performance state estimator. It can observe low-frequency perturbation accurately because of its mathematical design. SPO is similar to extended state observer (ESO) [18,19]. Both algorithm estimates not only system states, but also perturbation, which can be further used for perturbation compensation or disturbance rejection.

Sliding mode control with sliding perturbation estimation (SMCSPO) is a fusion of SMC and SPO, which utilizes only partial state feedback to estimate the system states and perturbation with reasonable accuracy. SMCSPO has good state estimation accuracy. This estimation of perturbation is useful in the reduction of chattering by using perturbation compensation techniques [2,3]. SMCSPO is a highly accurate control scheme for the estimation of state and perturbation in control of surgical robots and hydraulic robot manipulators [20–23]. The purpose of this estimation is used to reduce the chattering from system output by perturbation compensation. However, in conventional sliding mode control, during the sliding phase, the gain K should be greater than the upper bound of perturbation in order to satisfy the Lyapunov stability criteria. The greater the value of gain K , the larger the chattering at the system output, which is a highly undesirable phenomena in mechanical systems. Different techniques have been applied to reduce chattering from SMC, like the introduction of a boundary layer and perturbation compensation techniques [3]. The greater value of gain K increases the breaking frequency of the low pass filter between the sliding surface and perturbation because the system becomes sensitive to high-frequency perturbation. SMCSPO is a robust control scheme for trajectory tracking and perturbation estimation, but its characteristics can be further improved by reducing the reaching time, decreasing the error from the system output, and making the system more insensitive from the incoming perturbation signal.

In this research, efficient control of a hydraulic non-linear robot manipulator with modified sliding mode control named proportional derivative sliding mode control with sliding perturbation observer (PDSMCSPO) is proposed to reduce more chattering from the output of conventional SMC. Chattering can be reduced by decreasing the value of the switching gain K for it to become more insensitive to high-frequency perturbation as compared with SMC. From the proposed controller with SPO, a more robust controller has been achieved, which reaches the desired state faster and has a better performance at reducing error as compared with SMCSPO. This proposed PDSMCSPO has reduced the convergence time, decreased the error from the output, and made the system more insensitive to the perturbation signal as compared with previous SMCSPO [24].

The manuscript is organized in this way: Section 2 of this paper presents the control theory and details the previous one, and our proposed scheme and their characteristics are discussed. Section 3 describes the simulation and experimental results of both schemes and their comparison are mentioned. Section 4 entails the concluding remarks to this study.

2. Control Design

In this section, 3 different types of controllers are discussed and compared including (SMCSPO, PDSMC and PDSMCSPO). Proportional derivative sliding mode control (PDSMC) is an improved controller with less chattering. SMCSPO and PDSMCSPO are more robust controllers with perturbation compensation. First, the system dynamics is defined. After that, SPO and its integration with SMC are

discussed, and our proposed scheme of PDSMC integrated with SPO is discussed. Finally, the last design procedure is described.

2.1. Dynamics of aHydraulic System

The hydraulic robot manipulator is shown in Figure 1. This system consists of two hydraulic operated links, and one link is servo motor operated. The last link of the robot manipulator is used for simulation and experimental purposes. The dynamics of this third link is extracted from the signal compression method [25] which used an equivalent compressed signal to identify the system’s linear parameters.

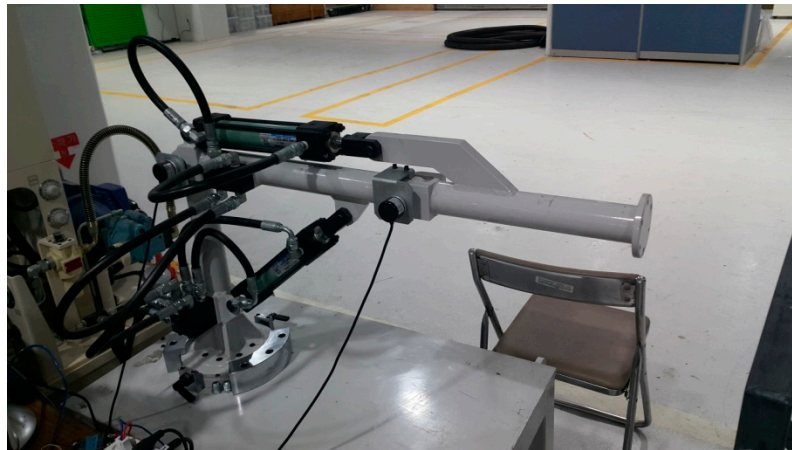


Figure 1. Hydraulic robot manipulator.

The schematic diagram of the third link of the robot manipulator is shown in Figure 2, and its mathematical model is shown below.

$$(J + \Delta J) \cdot \ddot{\theta} + (B + \Delta B + \varphi) \cdot \dot{\theta} + 0.5 \cdot M \cdot g \cdot L \cdot \sin\theta + D = F \cdot L \tag{1}$$

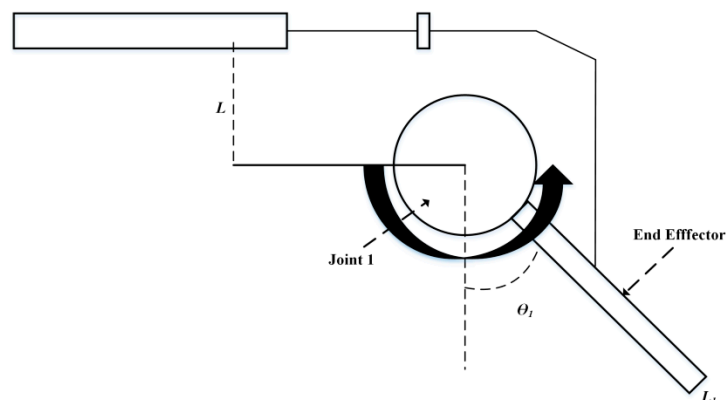


Figure 2. Third link schematic diagram.

In the equation above, F is the force applied by the hydraulic cylinder, L is the length of the link, J and ΔJ are inertia terms and their uncertainty, whereas B and ΔB are damper terms and its uncertainty. D is the external disturbance of the environment. φ is the viscosity term of the cylinder. The perturbation is defined below:

$$\psi = \Delta J + \Delta B + D + \varphi \tag{2}$$

After solving further, the following equation is obtained:

$$\ddot{\theta} = \frac{1}{J}(u - B * \dot{\theta} + \psi) \tag{3}$$

where ψ is the perturbation which is defined in Equation (2). The other parameters of Equation (1) were identified by the signal compression method. The values of the linear parameters are shown below in Table 1.

Table 1. Hydraulic link parameters.

Serial No	Moment of Inertia (kg·m ²)	Damper (kg·m ² /s)
1	303	15,355

2.2. Sliding Mode Control with Sliding Perturbation Observer (SMCSPO)

In this section, the control theory of SMCSPO is explained in detail. First, the structure of the sliding perturbation observer (SPO) is explained, then the integration of the SMC and SPO, mentioned above, is discussed.

2.2.1. Sliding Perturbation Observer (SPO)

SPO is a non-linear observer that uses partial state feedback (position) to estimate the system states and perturbation [1]. The structure of the second order system can be presented as:

$$\begin{aligned} \dot{x}_{1j} &= x_{2j} \\ \dot{x}_{2j} &= f_j(x) + \sum_{i=1}^n b_{ji}(x)u_i + \psi_j(x, t) \end{aligned} \tag{4}$$

where $\psi_j(x, t)$ is the perturbation which is defined in Equation (2). Where $X = [x_1 x_2]^T$ is the state vector and x_1 is the only measurable state of encoder data from the hydraulic link joint (system output). The observer’s function was to estimate state vector X despite uncertainties. The term $f_j(x)$ corresponds to non-linear driving terms. So the estimation state of the system is defined as:

$$\begin{aligned} \dot{\hat{x}}_{1j} &= \hat{x}_{2j} \\ \dot{\hat{x}}_{2j} &= f_j(\hat{x}) + \sum_{i=1}^n b_{ji}(\hat{x})u_i + \hat{\psi}(\hat{x}, t) \end{aligned} \tag{5}$$

where $\hat{\psi}_j(\hat{x}, t)$ is the estimated perturbation. Before integrating the sliding observer into SMC, it was convenient to decouple the control variable using the following transformation [2], as shown below:

$$f_j(\hat{x}) + \sum_{i=1}^n b_{ji}(\hat{x})u_i = \alpha_{3j} \cdot \bar{u}_j \tag{6}$$

In above Equation (6), α_3 is a positive constant and \bar{u} is a new control variable. \bar{u} has the same unit as the control input u (N.m).

The control input u can be defined as:

$$u = B^{-1} \text{col}[\alpha_3 \cdot \bar{u} - f_j(\hat{x})] \tag{7}$$

where $u = [u_1 \dots u_n]^T$ and $B = [b_{ji}(\hat{x})]_{n \times n}$ are control input vectors, and Col means column vector. The difference $b_{ji}(\hat{x}) - b_{ji}(x)$ is considered as a part of the term Δb_{ji} in Equation (2). Equation (7) allows the system dynamics to be rewritten as:

$$\ddot{x}_1 = \alpha_3 \cdot \bar{u} + \psi_j. \tag{8}$$

A new state variable was introduced to estimate the perturbation and the relation between this new variable and perturbation is shown in the following equation:

$$x_{3j} = \alpha_{3j} \cdot x_{2j} - \frac{\psi_j}{\alpha_{3j}} \tag{9}$$

The derivative of the above relation is shown below:

$$\dot{x}_{3j} = \alpha_{3j} \cdot \dot{x}_{2j} - \frac{\dot{\psi}_j}{\alpha_{3j}} \tag{10}$$

We assume that the constant α_3 is selected as a larger value such that $\frac{\dot{\psi}_j}{\alpha_3}$ becomes negligible as compared with other terms in the equation. The sliding perturbation observer (SPO) equations can be described as:

$$\begin{aligned} \dot{\hat{x}}_1 &= \hat{x}_2 - k_1 \cdot \text{sat}(\tilde{x}_1) - \alpha_1 \cdot \tilde{x}_1 \\ \dot{\hat{x}}_2 &= -k_2 \cdot \text{sat}(\tilde{x}_1) + \alpha_3 \cdot \bar{u} - \alpha_2 \cdot \tilde{x}_1 \end{aligned} \tag{11}$$

$$\begin{aligned} \dot{\hat{x}}_3 &= \alpha_3^2 \cdot (\alpha_3 \cdot \hat{x}_2 + \bar{u} - \hat{x}_3) \\ \hat{\psi} &= \alpha_3(\alpha_3 \cdot \hat{x}_2 - \hat{x}_3) \end{aligned} \tag{12}$$

where $k_1, k_2, \alpha_3, \alpha_1, \alpha_2$ are constant and their values are greater than 0 and $\text{sat}(\hat{x}_1)$ is the saturation function which is defined below.

$$\text{sat}(\tilde{x}_1) = \begin{cases} \frac{\tilde{x}_1}{|\tilde{x}_1|} & \text{if } |\tilde{x}_1| > \varepsilon_0 \\ \frac{\tilde{x}_1}{\varepsilon_0} & \text{if } |\tilde{x}_1| \leq \varepsilon_0 \end{cases} \tag{13}$$

where $\tilde{x}_1 = \hat{x}_1 - x_1$ is the state estimation error and ε_0 is the boundary layer of the sliding observer.

It is assumed that the observer starts at the sliding surface and remains when time ($t = 0$) $\tilde{x}_1 = 0, \tilde{x}_2 = 0$. To fulfill this assumption, the gain k_2 should be greater than the perturbation ($k_2 > \psi(x, t)$). Because of this, the attractive damping coefficient becomes zero.

The observer state error dynamics become:

$$\begin{aligned} \dot{\tilde{x}}_1 &= \tilde{x}_2 - \left(\frac{k_1}{\varepsilon_0}\right) \cdot \tilde{x}_1 \\ \dot{\tilde{x}}_2 &= -\left(\frac{k_2}{\varepsilon_0}\right) \cdot \tilde{x}_1 + \tilde{\psi} \\ \dot{\tilde{x}}_3 &= \alpha_3^2(-\tilde{x}_3 + \alpha_3 \cdot \tilde{x}_2) + \frac{\dot{\psi}}{\alpha_3}. \end{aligned} \tag{14}$$

During the sliding phase, the relation between the state estimation error and perturbation estimation error is a low pass filter as shown,

$$\frac{\tilde{x}_2}{\tilde{\psi}} = \frac{1}{p + \frac{k_2}{k_1}} \tag{15}$$

The relation between the state estimation error \tilde{x}_2 and the actual perturbation is derived as shown below which is a low pass filter.

$$\frac{\tilde{x}_2}{\psi} = \frac{p\left(p + \frac{k_1}{\varepsilon_0}\right)}{p^3 + p^2 \cdot \left(\frac{k_1}{\varepsilon_0}\right) + p \cdot \left(\frac{k_2}{\varepsilon_0}\right) + \left(\frac{k_2}{\varepsilon_0}\right) \cdot \alpha_3^2} \tag{16}$$

2.2.2. Integration of SMC and SPO (SMCSPO)

Integration of SMC into SPO generates SMCSPO [1] which is a robust control against perturbation. SMCSPO uses a perturbation compensation technique. It is a combination of a controller and observer;

it estimates the system states and perturbation and uses that information to control an uncertain system. An estimated sliding surface is defined as:

$$\hat{s} = \dot{\hat{e}} + c \cdot \hat{e} \tag{17}$$

where $\hat{e} = \hat{x}_1 - x_d$ is the estimated error and c is a constant value greater than 0.

The estimated error of the sliding surface is shown below.

$$\tilde{s} = \hat{s} - s \tag{18}$$

The estimated error of a sliding surface is computed as:

$$\tilde{s} = \tilde{\hat{x}}_1 + c \cdot \tilde{\hat{x}}_1 \tag{19}$$

The control \bar{u} is selected such that it satisfies the following condition during the reaching phase.

$$\hat{s} \cdot \dot{\hat{s}} \leq 0 \tag{20}$$

For the above condition, the $\dot{\hat{s}}$ dynamic is selected as shown below.

$$\dot{\hat{s}} = -K \cdot \text{sat}(\hat{s}) \tag{21}$$

The definition of $\text{sat}(\hat{s})$ is defined as:

$$\text{sat}(\hat{s}) = \begin{cases} \frac{\hat{s}}{|\hat{s}|} & \text{if } |\hat{s}| > \varepsilon_c \\ \frac{\varepsilon_c}{\hat{s}} & \text{if } |\hat{s}| \leq \varepsilon_c \end{cases} \tag{22}$$

After taking the derivative of Equation (17) and using Equation (11), we get the following equation:

$$\dot{\hat{s}} = \alpha_3 \cdot \bar{u} - \tilde{x}_1 \left\{ \frac{k_2}{\varepsilon_0} + \frac{c \cdot k_1}{\varepsilon_0} - \frac{k_1^2}{\varepsilon_0^2} \right\} - \frac{k_1}{\varepsilon_0} \tilde{x}_2 + c(\hat{x}_2 - \dot{x}_d) - \ddot{x}_d + \hat{\psi} \tag{23}$$

In Equation (23), it is assumed that $\tilde{x}_2 = 0$ to enforce Equation (20).

After putting the value of $\dot{\hat{s}}$ in Equation (21), we get the following control input \bar{u} .

$$\bar{u} = \frac{1}{\alpha_3} \left[-K \cdot \text{sat}(\hat{s}) + \tilde{x}_1 \left\{ \frac{k_2}{\varepsilon_0} + \frac{c \cdot k_1}{\varepsilon_0} - \frac{k_1^2}{\varepsilon_0^2} \right\} + \ddot{x}_d - c(\hat{x}_2 - \dot{x}_d) - \hat{\psi} \right] \tag{24}$$

After substituting Equation (24) into Equation (23), the resulting dynamics $\dot{\hat{s}}$ have the effect of state estimation error as shown.

$$\dot{\hat{s}} = -K \cdot \text{sat}(\hat{s}) - \frac{k_1}{\varepsilon_0} \tilde{x}_2 \tag{25}$$

The above relation shows that during the reaching phase, the $\dot{\hat{s}}$ dynamics are affected by the estimation error of state \tilde{x}_2 . To enforce the condition of Equation (20), the following condition should be fulfilled.

$$K > \frac{k_1^2}{\varepsilon_0} \tag{26}$$

As we know that $|\tilde{x}_2| \leq k_1$.

When the system reached the sliding surface or prescribed manifold $|\hat{s}| \leq \varepsilon_c$, the actual s dynamics was obtained as shown below.

$$\dot{s} + \frac{K}{\varepsilon_c} s = \tilde{x}_1 \left\{ \frac{k_2}{\varepsilon_0} - \left(\frac{k_1}{\varepsilon_0} - \frac{K}{\varepsilon_c} \right) \left(c - \frac{k_1}{\varepsilon_0} \right) \right\} - \tilde{x}_2 \left\{ \frac{K}{\varepsilon_c} + c \right\} - \hat{\psi} \tag{27}$$

2.3. PD Sliding Mode Control (PDSMC)

In this section, the details of the proposed scheme are discussed, and in the next section, the proposed scheme is integrated with SPO to achieve robust control with faster convergence and better characteristics as compared with SMCSPPO.

As the main idea was to generate a sliding surface which was the sum of the derivative and proportional gain of PID control or to introduce the derivative gain in the structure of the sliding surface as shown below.

$$s = k_d \cdot \dot{e} + k_p \cdot e \tag{28}$$

k_p & k_d are the proportional and derivative gain where e is the error as defined in the above section.

The value of $k_p > 0$, $0 < k_d < 1$. In PDSMC, during the reaching phase, the \dot{s} dynamics is shown below.

$$\dot{s} = -K' \cdot \text{sat}(s) + k_d \cdot \psi \tag{29}$$

In order to fulfill the sliding condition $s \cdot \dot{s} \leq 0$ the gain K' should be greater than the $k_d \cdot \psi$ as shown below.

$$K' > k_d \cdot \psi \tag{30}$$

As it can be seen in Equation (30) that during the reaching phase, the gain k_d multiplied with perturbation and reduced the effect of perturbation because the value of this gain was $k_d < 1$, but greater than 0. Because of this small value of switching gain, Small K' was required as compared with conventional SMC switching gain K . This reduced chattering from the system output and its sliding surface. When the system reached the sliding surface, or within the boundary layer, the \dot{s} dynamics become as shown below.

$$\dot{s} = -\frac{K'}{\epsilon_c} s + k_d \cdot \psi \tag{31}$$

After taking the Laplace transform, the transfer function of the sliding surface over perturbation is obtained as shown below.

$$\frac{s}{\psi} = \frac{k_d}{p + \frac{K'}{\epsilon_c}} \tag{32}$$

The above equation is a low pass filter between the sliding surface and perturbation, with breaking frequency $\frac{K'}{\epsilon_c}$.

Consider a mass damper system as Equation (3). After taking the derivative of Equation (28) and substituting Equation (3) into it, the following relation was obtained.

$$\dot{s} = k_d \left\{ \frac{1}{J} [u - B \cdot \dot{x} - \psi] - \ddot{x}_d \right\} + k_p \cdot \dot{e} \tag{33}$$

As we know that to fulfill the sliding condition $s \cdot \dot{s} \leq 0$. \dot{s} should be equal to $\dot{s} = -K \cdot \text{sat}(s)$

$$k_d \left\{ \frac{1}{J} [u - B \cdot \dot{x} - \psi] - \ddot{x}_d \right\} + k_p \cdot \dot{e} = -K \cdot \text{sat}(s) \tag{34}$$

After rearranging the above equation, the following controller output is obtained for PDSMC.

$$u = -\frac{J \cdot K \cdot \text{sat}(s)}{k_d} + J \cdot \ddot{x}_d - \frac{J \cdot k_p \cdot \dot{e}}{k_d} + B \cdot \dot{x} \tag{35}$$

2.3.1. Proposed Scheme Characteristics

The proposed logic outperformed conventional SMC as:

- a. *Less Chattering*

In our proposed scheme during the reaching phase, the gain k_d was multiplied with perturbation ψ and reduced the effect of perturbation more than conventional SMC. That's why in PDSMC, a small switching gain K' was required as compared with conventional SMC gain K . Due to the large gain K in SMC, the chattering was observed in the output of SMC, whereas there was small chattering in PDSMC.

b. Insensitive to High Frequency Perturbation

When the system reached the sliding surface, or was inside the boundary layer $|s| \leq \epsilon_c$, a transfer function which was a low pass filter between the sliding surface and perturbation was obtained in PDSMC. The breaking frequency of this filter $\frac{K'}{\epsilon_c}$, was smaller than the breaking frequency $\frac{K}{\epsilon_c}$ of conventional SMC ($K' < K$). This meant that during the sliding phase, our proposed scheme was insensitive to the high-frequency perturbation signal.

The two points mentioned above are the advantages of PDSMC. In the next section, PDSMC is integrated with SPO, and its characteristics will be compared with conventional SMC/SPO.

2.3.2. Integration of PDSMC and SPO (PDSMC/SPO)

This section presents the integration of PDSMC with the sliding perturbation and (SPO). The fusion PDSMC with SPO generated a new robust control algorithm, PDSMC/SPO, with perturbation compensation. This PDSMC/SPO utilized only partial state feedback (position) to estimate the velocity and perturbation and utilizing this information to control the system.

$$\hat{s} = k_d \cdot \dot{\hat{e}} + k_p \cdot \hat{e} \tag{36}$$

In the relation above, $\hat{e} = \hat{x} - x_d$ was the estimated error. k_p & k_d were proportional and the derivative gain of the proportional-integral-derivative controller (PID). It was assumed that $k_p > 1$, $0 < k_d < 1$. The actual sliding surface is defined as below.

The estimated error of the sliding surface is shown below.

$$\tilde{s} = \hat{s} - s \tag{37}$$

By using Equation (28) and Equation (36) it can be computed as

$$\tilde{s} = k_d \cdot \dot{\tilde{x}}_1 + k_p \cdot \tilde{x}_1 \tag{38}$$

The control \bar{u} was selected such that it satisfied the condition $\hat{s} \cdot \dot{\hat{s}} \leq 0$ during the reaching phase. To satisfy this condition, $\dot{\hat{s}}$ should be equal to $\dot{\hat{s}} = -K \cdot sat(\hat{s})$. After taking the derivative of Equation (36) and using Equation (11), the following equation was obtained.

$$\begin{aligned} \dot{\hat{s}} = k_d \cdot \alpha_3 \cdot \bar{u} - \tilde{x}_1 \left\{ \frac{k_d \cdot k_2}{\epsilon_o} + \frac{k_p \cdot k_1}{\epsilon_o} - \frac{k_d \cdot k_1^2}{\epsilon_o} \right\} - \left\{ \frac{k_d \cdot k_1}{\epsilon_o} \right\} \tilde{x}_2 \\ + k_p \{ \hat{x}_2 - \dot{x}_d \} - k_d \cdot \ddot{x}_d + k_d \cdot \hat{\psi} \end{aligned} \tag{39}$$

In Equation (39) above, it was assumed that $\tilde{x}_2 = 0$ to enforce Equation (20). After putting the value of \hat{s} in Equation (21), we get the following control input \bar{u} .

$$\bar{u} = \frac{1}{\alpha_3} \left[-\frac{K'}{k_d} sat(\hat{s}) + \tilde{x}_1 \left\{ \frac{k_p \cdot k_1}{k_d \cdot \epsilon_o} + \frac{k_2}{\epsilon_o} - \frac{k_1^2}{\epsilon_o} \right\} - \frac{k_p}{k_d} \{ \hat{x}_2 - \dot{x}_d \} - \hat{\psi} + \ddot{x}_d \right] \tag{40}$$

After substituting Equation (40) into Equation (39), the resulting $\dot{\hat{s}}$ dynamics had the effect of state estimation error as shown, but this time, the derivative gain was multiplied with this error and reduced the effect on the $\dot{\hat{s}}$ dynamics because the value of this gain, k_d , was less than unity.

$$\dot{\hat{s}} = -\frac{K'}{\varepsilon_c} \cdot \hat{s} - \frac{k_d \cdot k_1}{\varepsilon_o} \cdot \tilde{x}_2 \tag{41}$$

In the equation above, it can be seen that during the reaching phase, the $\dot{\hat{s}}$ dynamics were affected by the state estimates error \tilde{x}_2 to enforce the sliding condition in Equation (20).

$$K' > \frac{k_d \cdot k_1^2}{\varepsilon_o} \tag{42}$$

When the system reached the sliding surface or the prescribed manifold $|\hat{s}| \leq \varepsilon_c$, the actual s dynamics were obtained as shown below by using Equation (37).

$$\dot{s} + \frac{K}{\varepsilon_c} s = \tilde{x}_1 \left\{ \frac{k_d \cdot k_2}{\varepsilon_o} - \left(\frac{K}{\varepsilon_c} - \frac{k_1}{\varepsilon_o} \right) \left(k_p - \frac{k_1 \cdot k_d}{\varepsilon_o} \right) \right\} - \tilde{x}_2 \left\{ \frac{K \cdot k_d}{\varepsilon_c} + k_p \right\} - k_d \cdot \tilde{\psi} \tag{43}$$

2.3.3. Design Procedure

This section presents the general design procedure for PDSCMSPO. When the condition $|\hat{s}| \leq \varepsilon_c$, $|\tilde{x}_1| \leq \varepsilon_o$ had been achieved, it was assumed that $c = \frac{K}{\varepsilon_c}$ and $c = \frac{k_p}{k_d}$. The controller and observer dynamics took place in the following form.

$$\begin{bmatrix} \dot{\tilde{x}}_1 \\ \dot{\tilde{x}}_2 \\ \dot{\tilde{x}}_3 \\ \dot{\hat{s}} \end{bmatrix} = \begin{bmatrix} \frac{-k_1}{\varepsilon_o} & 1 & 0 & 0 \\ \frac{-k_2}{\varepsilon_o} & \alpha_3^2 & -\alpha_3 & 0 \\ 0 & \alpha_3 & -\alpha_3^2 & 0 \\ \frac{k_d k_2}{\varepsilon_o} - \left(\frac{K}{\varepsilon_c} - \frac{k_1}{\varepsilon_o} \right) \left(k_p - \frac{k_1 \cdot k_d}{\varepsilon_o} \right) & \left(\frac{K \cdot k_d}{\varepsilon_o} + k_p + \alpha_3^2 \right) & k_d \cdot \alpha_3 & \frac{-K}{\varepsilon_c} \end{bmatrix} \begin{bmatrix} \tilde{x}_1 \\ \tilde{x}_2 \\ \tilde{x}_3 \\ s \end{bmatrix} + \begin{bmatrix} 0 \\ 0 \\ 1 \\ 0 \end{bmatrix} \frac{\dot{\psi}}{\alpha_3} \tag{44}$$

It appears like a conventional Luenberger observer and for the stability satisfaction we used the pole placement technique. The characteristic equation of the matrix above is shown below.

$$\left[\lambda + \frac{K}{\varepsilon_c} \right] \left[\lambda^3 + \left(\frac{k_1}{\varepsilon_o} \right) \lambda^2 + \left(\frac{k_2}{\varepsilon_o} \right) \lambda + \alpha_3^2 \left(\frac{k_2}{\varepsilon_o} \right) \right] = 0 \tag{45}$$

And the desired 4th order polynomial equation is given below.

$$(s + \lambda_d)^4 = s^4 + 4 \cdot s^3 \cdot \lambda_d + 6 \cdot s^2 \cdot \lambda_d^2 + 4 \cdot s \cdot \lambda_d^3 + \lambda_d^4 \tag{46}$$

Comparing the coefficients of Equations (45) and (46), we get the following set of equations.

$$\frac{k_1}{\varepsilon_o} = 3\lambda_d, \frac{k_2}{\varepsilon_o} = \lambda_d, \alpha_3 = \sqrt{\frac{\lambda_d}{3}}, \frac{K}{\varepsilon_c} = \lambda_d, \frac{k_p}{k_d} = \lambda_d \tag{47}$$

From the structure of SPO, the relation between estimated perturbation and actual perturbation was derived as shown below, which was a low pass filter between estimated perturbation and actual perturbation with breaking frequency λ_d .

$$\frac{\hat{\psi}}{\psi} = \frac{\lambda_d^3}{(p + \lambda_d)^3} \tag{48}$$

A large value of λ_d increased the accuracy of perturbation estimation. Better perturbation estimation accuracy meant better system performance. The Bode plot of the relation above can be seen

in Figure 3. The red line (dotted) is when $\lambda_d = 30$ (15 rad/s breaking frequency) and the blue line $\lambda_d = 30$ (25 rad/s).

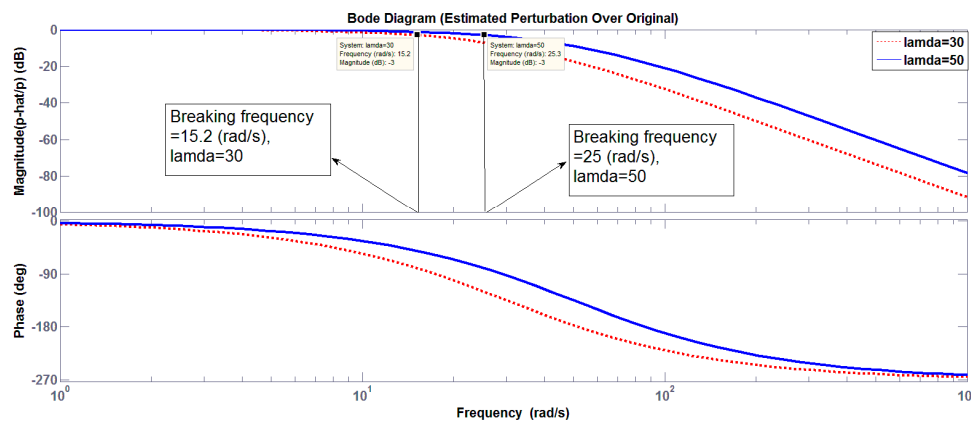


Figure 3. Bode plot of estimated perturbation over original perturbation.

2.3.4. Proposed Scheme Characteristics

a. Attenuation of Perturbation Signal During the Sliding Phase.

The transfer function between the sliding surface and perturbation for both control schemes for our proposed one (PDSMCSPO) Equation (49) and conventional (SMCSPO) one Equation (50) are shown below.

$$\frac{s}{\psi} = \frac{k_d \cdot p^3 + p^2(k_p + 4 \cdot k_d \cdot \lambda_d) + p(k_p \cdot \lambda_d + 9 \cdot \lambda_d^2 \cdot k_d)}{(p + \lambda_d)^4} \tag{49}$$

$$\frac{s}{\psi} = \frac{p^3 + 5 \cdot \lambda_d \cdot p^2 + 10 \cdot \lambda_d^2 \cdot p}{(p + \lambda_d)^4} \tag{50}$$

In Figure 4, the red line is the Bode plot of SMCSPO and the blue line (dotted) is for PDSMCSPO. It can be seen that our proposed logic attenuated the incoming perturbation signal better as compared to SMCSPO during the sliding phase. The value of lambda is 30 for both schemes.

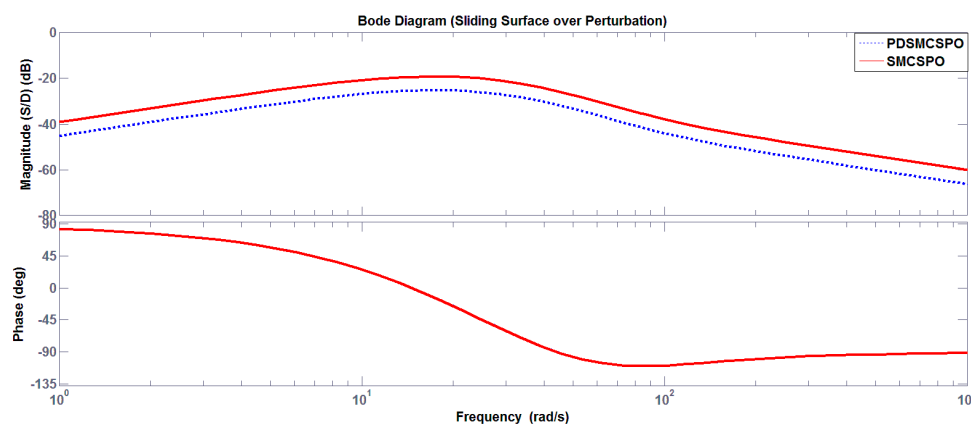


Figure 4. Bode plot of sliding surface over perturbation.

b. Small Output Error

This robust control PDSMCSPO had small output error compared with conventional SMCSPO because this scheme attenuated the perturbation signal more than conventional SMCSPO. Figure 3 is the Bode plot between the error and perturbation. It can be seen that PDSMCSPO attenuated

perturbation more than SMCSPO. The transfer function between error and perturbation for both schemes, PDSMCSPO Equation (51), and SMCSPO Equation (52) are shown below.

$$\frac{e}{\psi} = \frac{k_d \cdot p^3 + p^2(k_p + 4 \cdot k_d \cdot \lambda_d) + p(k_p \cdot \lambda_d + 9 \cdot \lambda_d^2 \cdot k_d)}{0.5 \cdot (p + \lambda_d)^5} \tag{51}$$

$$\frac{e}{\psi} = \frac{p^3 + 5 \cdot \lambda_d \cdot p^2 + 10 \cdot \lambda_d^2 \cdot p}{(p + \lambda_d)^5} \tag{52}$$

In Figure 5, the blue line (dotted), PDSMCSPO, has more attenuation capability than the red line, SMCSPO. The value of lambda = 30.

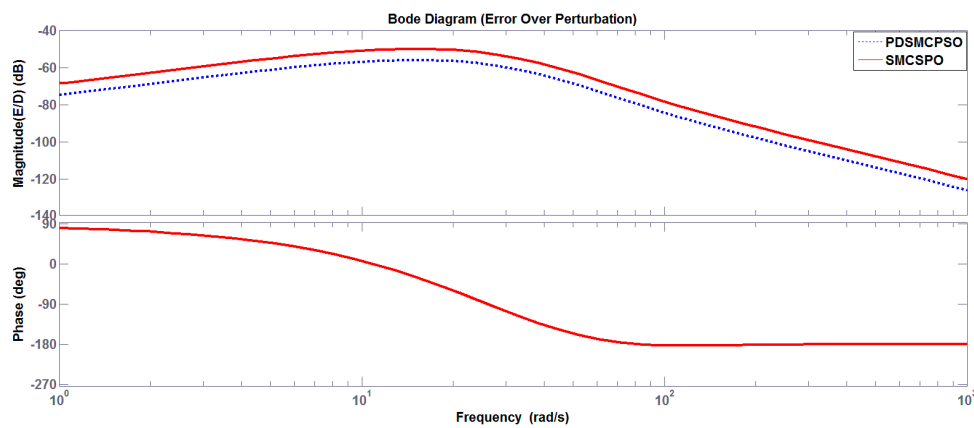


Figure 5. Bode plot of error over perturbation.

c. *Faster Convergence.*

Our proposed scheme had faster convergence to the desired state as compared with conventional SMCSPO. The reaching time can be calculated as:

$$t_r \leq \frac{s_0}{\eta} \tag{53}$$

η is a constant which can be defined as:

$$K = \eta + \psi \tag{54}$$

Step input is given to the system.

i. *SMCSPO*

From Equation (17).

$$\hat{s} = \dot{\hat{e}} + c \cdot \hat{e}$$

In case of step input $r = 1, y = 0, \dot{y} = 0, \dot{r} = 0$.

$$\hat{s}_0 = \dot{r} - \dot{\hat{y}} + c(r - \hat{y}) \tag{55}$$

$\dot{r} = 1, \dot{\hat{y}} = 0, \hat{y} = 0$ at time $t = 0$.

So Equation (55) becomes:

$$\hat{s}_0 = c \tag{56}$$

$$t_r \leq \frac{c}{\eta} \tag{57}$$

ii. *PDSMCSPO*

From Equation (36)

$$\hat{s} = k_d \cdot \dot{\hat{e}} + k_p \cdot \hat{e}$$

In case of step $\dot{r} = 1, \dot{\hat{y}} = 0, \hat{y} = 0$ at time $t = 0$.

$$\hat{s} = k_d(\dot{r} - \dot{\hat{y}}) + k_p(r - \hat{y}) \tag{58}$$

Equation (58) above becomes:

$$\hat{s} = k_p \tag{59}$$

And it is known that $k_p < c$ so that the reaching time is smaller in PDSMCSPO.

3. Simulation and Experimental Results

In this section, the simulation and experimental results are shown. A mass damper system was considered for simulation, and an experiment was conducted on the link of the hydraulic robot manipulator.

3.1. Simulation Results of SMC and PDSMC

In this section, simulation results of SMC and PDSMC are presented. Parameter values can be seen in Table 2. In the simulation, we considered external disturbance a constant value (500) and the parameters of the system were selected on the basis of this disturbance. As discussed earlier, the gain K should be greater than the upper bound of perturbation in Equation (9). That's why the value of switching gain $K = 550$ (SMC) was greater than disturbance 500. In the PDSMC case, the gain $K' = 275$ follows Equation (44).

Table 2. SMC and PDSMC paramters.

Serial. NO	SMC	PDSMC
1	$K = 550$	$K = 275$
2	$C = 16$	$k_p = 8, k_d = 0.5$
3	$D = 500$	$D = 500$
4	Step input	Step input

Step input was given to the system and the following results were observed.

3.1.1. Step Output

Chattering was observed in the output of SMC whereas the PDSMC output had less chattering which can be seen in Figure 6. The solid red line shows the output of SMC which has chattering effects and the dotted blue line shows the output of PDSMC which has a small amount of chattering. As mentioned earlier, the switching gain K of PDSMC was smaller than SMC.

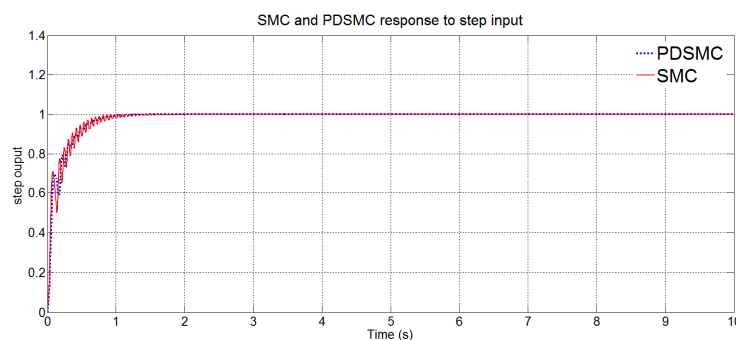


Figure 6. Sliding mode control (SMC) and proportional derivative sliding mode control (PDSMC) output response against step input.

3.1.2. Sliding Surface Response

Figure 7 shows the sliding surface behavior of both controller schemes. It can be seen that there was a big overshoot in SMC (red line) as compared to PDSMC (blue line), which had smaller overshoot. Chattering was also in the sliding surface of SMC (solid red line), and on the other side, PDSMC had a small amount of chattering.

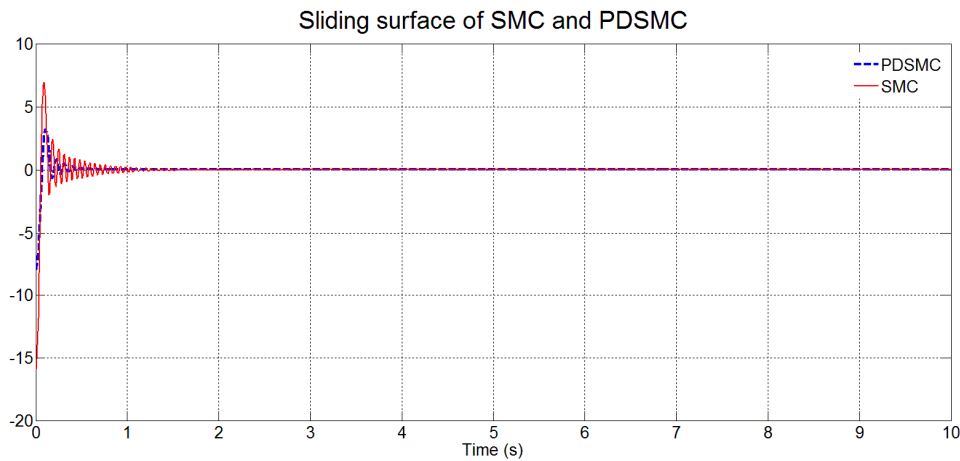


Figure 7. Sliding surface response of both schemes.

3.1.3. Low Pass Filter Characteristics

It was mentioned in the previous chapter that PDSMC had low pass filter characteristics compared with SMC because the breaking frequency of PDSMC is smaller than SMC. It emphasized that during the sliding phase, when PDSMC was insensitive to high-frequency perturbation compared to conventional SMC. In Figure 8, the breaking frequency of SMC was 550 (rad/s, blue line), whereas the breaking frequency of PDSMC was 275 (rad/s, red line).

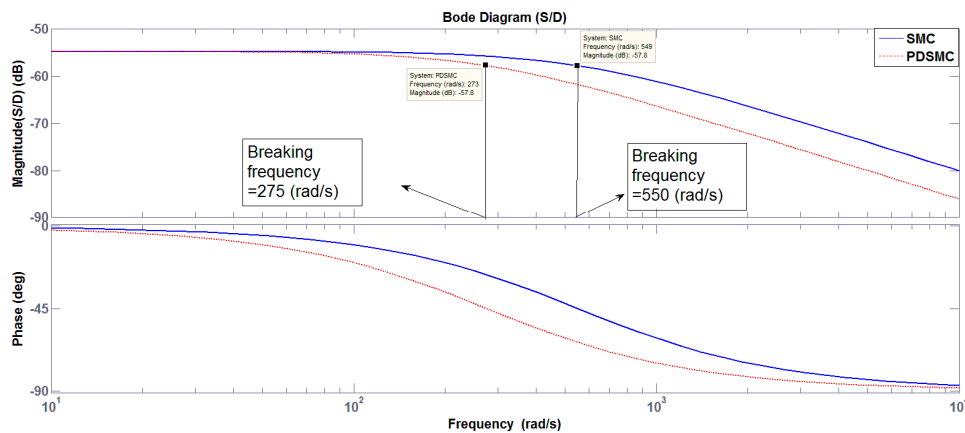


Figure 8. Bode plot of sliding surface over perturbation.

To understand this phenomenon, the following scheme was made. External sine wave disturbances of different frequencies were introduced in the simulation, and the effect of this disturbance was observed on the sliding surface.

Case 1

An external sine wave whose frequency was 50 (rad/s) was introduced in the simulation. It was observed that this frequency was less than the breaking frequency of both controllers, so it affected the sliding surface of both controllers. Figure 9 shows the effect of disturbance on both sliding surfaces.

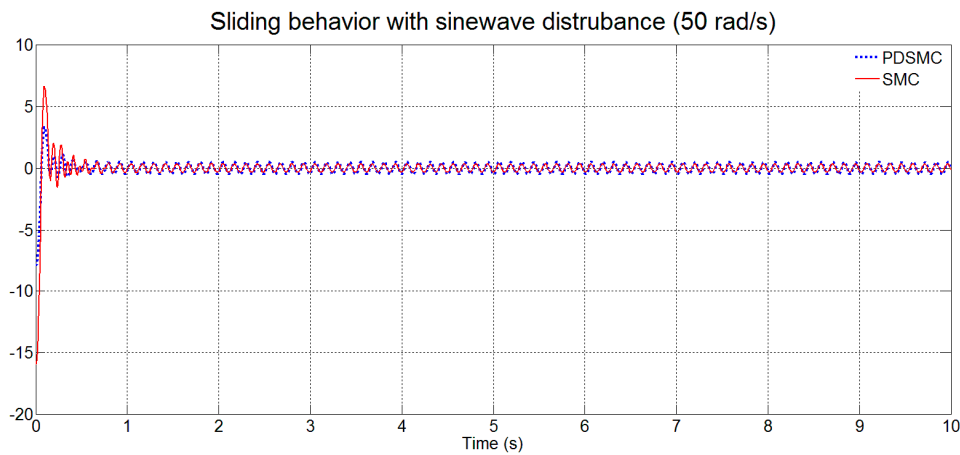


Figure 9. Effect of disturbance on sliding surface.

Case 2

The sine wave disturbance of frequency 300 (rad/s) was introduced since we know that the breaking frequency of SMC was 550 (rad/s) and PDSMC 275 (rad/s). This disturbance frequency was less than the breaking frequency of SMC, so it affected the SMC sliding surface whereas it did not affect PDSMC. In Figure 10, chattering is visible in the solid red line (SMC), whereas the sliding surface of PDSMC (dotted blue line) has no chattering during the sliding phase.

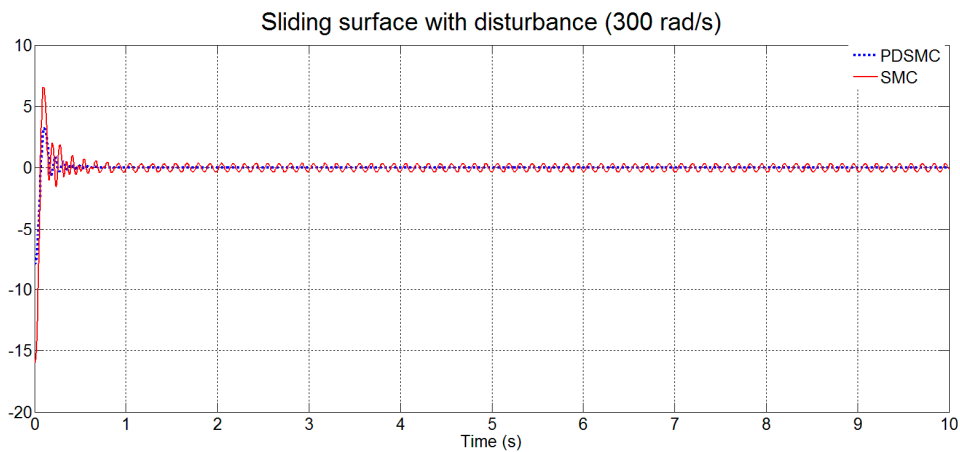


Figure 10. Effect of disturbance on sliding surface.

Case 3

In this case, disturbance frequency was greater than the breaking frequency of both controllers, so it did not affect the sliding surface of both schemes as shown in Figure 11.

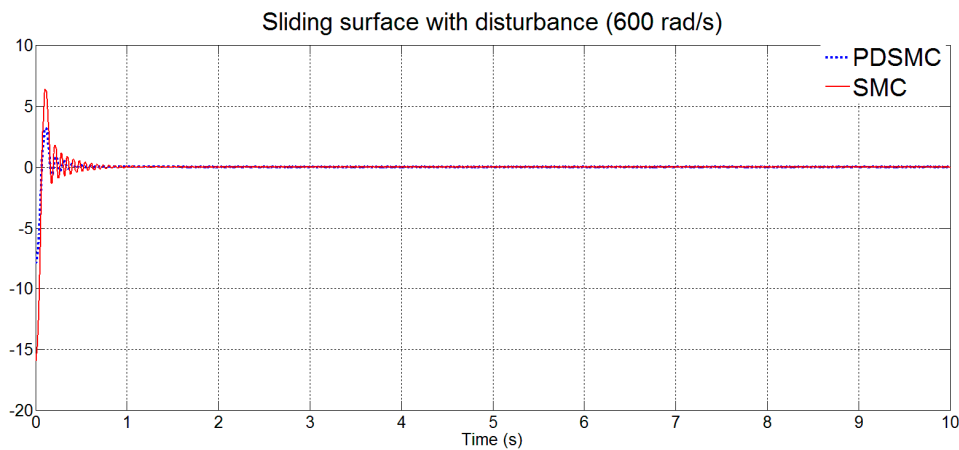


Figure 11. Effect of disturbance on sliding surface.

Table 3 below summarizes the whole phenomena.

Table 3. Effect of different frequency disturbances in sliding surface.

Serial. No	SMC	PDSMC	Disturbance
1	affected	affected	$D < 275$ (rad/s)
2	affected	not affected	$275 < D < 550$
3	not affected	not affected	$D > 550$

3.2. Simulation Results of SMCSPO and PDSMCSPO

In this section simulation results of both robust control schemes with perturbation compensation are presented.

3.2.1. SMCSPO

The control input to the system in the case of SMCSPO is shown below.

$$u_{smcspo} = J \cdot \alpha_3 \cdot \bar{u} + D \cdot \hat{x}_2 \tag{60}$$

where \bar{u} is defined as $|\hat{s}| > \epsilon_c$

$$\bar{u} = \frac{1}{\alpha_3} \left[-K \cdot \text{sat}(\hat{s}) + \tilde{x}_1 \left\{ \frac{k_2}{\epsilon_o} + \frac{c \cdot k_1}{\epsilon_o} - \frac{k_1^2}{\epsilon_o} \right\} - c(x_2 - \dot{x}_d) - \hat{\psi} + \ddot{x}_d \right] \tag{61}$$

When $|\hat{s}| \leq \epsilon_c$

$$\bar{u} = \frac{1}{\alpha_3} \left[-\frac{K \cdot \hat{s}}{\epsilon_c} + \tilde{x}_1 \left\{ \frac{k_2}{\epsilon_o} + \frac{c \cdot k_1}{\epsilon_o} - \frac{k_1^2}{\epsilon_o} \right\} - c \cdot (\hat{x}_2 - \dot{x}_d) - \hat{\psi} + \ddot{x}_d \right] \tag{62}$$

3.2.2. PDSMCSPO

The control input to the system in the case of PDSMCSPO is shown below.

When $|\hat{s}| > \epsilon_c$

$$\bar{u} = \frac{1}{\alpha_3} \left[-\frac{K'}{k_d} \text{sat}(\hat{s}) + \tilde{x}_1 \left\{ \frac{k_p \cdot k_1}{k_d \cdot \epsilon_o} + \frac{k_2}{\epsilon_o} - \frac{k_1^2}{\epsilon_o} \right\} - \frac{k_p}{k_d} (\hat{x}_2 - \dot{x}_d) - \hat{\psi} + \ddot{x}_d \right] \tag{63}$$

When $|\hat{s}| \leq \varepsilon_c$

$$\bar{u} = \frac{1}{\alpha_3} \left[-\frac{K' \cdot \hat{s}}{k_d \cdot \varepsilon_c} + \tilde{x}_1 \left\{ \frac{k_p \cdot k_1}{k_d \cdot \varepsilon_o} + \frac{k_2}{\varepsilon_o} - \frac{k_1^2}{\varepsilon_o} \right\} - \frac{k_p}{k_d} (\hat{x}_2 - \dot{x}_d) - \hat{\psi} + \ddot{x}_d \right] \tag{64}$$

System parameters for both schemes are shown in Table 4.

Table 4. Parameters.

Serial. No	SMCSPO	PDSMCSPO
1	$\lambda = 30$	$\lambda = 30$
2	$\varepsilon_o, \varepsilon_c = 1$	$\varepsilon_o, \varepsilon_c = 1$
3	$\frac{k_1}{\varepsilon_o} = 90$	$\frac{k_1}{\varepsilon_o} = 90$
4	$\frac{k_2}{\varepsilon_o} = 2700$	$\frac{k_2}{\varepsilon_o} = 2700$
5	$\alpha_3 = 3.16$	$\alpha_3 = 3.16$
6	$\frac{K}{\varepsilon_c} = 30$	$\frac{K}{\varepsilon_c} = 30$
7	$\frac{k_p}{k_d} = 30, k_d = 0.5, k_p = 15$	$c = \frac{k_p}{k_d} = 30$
8	Input = step	Input = step

3.2.3. Step Output

Step input was given to the system to observe the results. It was observed that the convergence of the output of PDSMCSPO was faster than SMCSPO. The reason was explained in the control theory chapter. In Figure 12, it is visible that the output response of PDSMCSPO (blue line) is faster than the SMCSPO (red line).

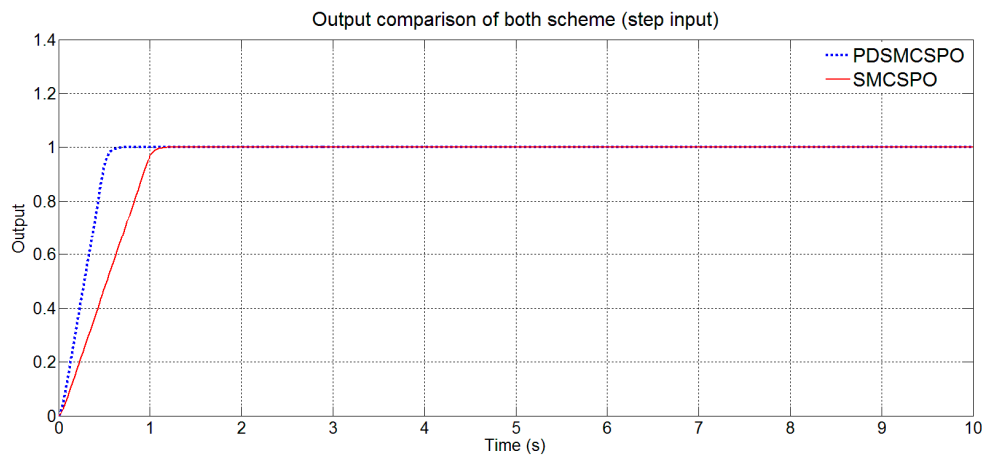


Figure 12. Output response of both schemes.

3.2.4. Sliding Surface Response

The convergence time of the sliding surface of PDSMCSPO was faster than SMCSPO. In Figure 13, it can be seen that the PDSMCSPO (blue line) sliding surface reached zero faster than SMCSPO (red line), and the starting point of PDSMCSPO was almost half of SMCSPO.

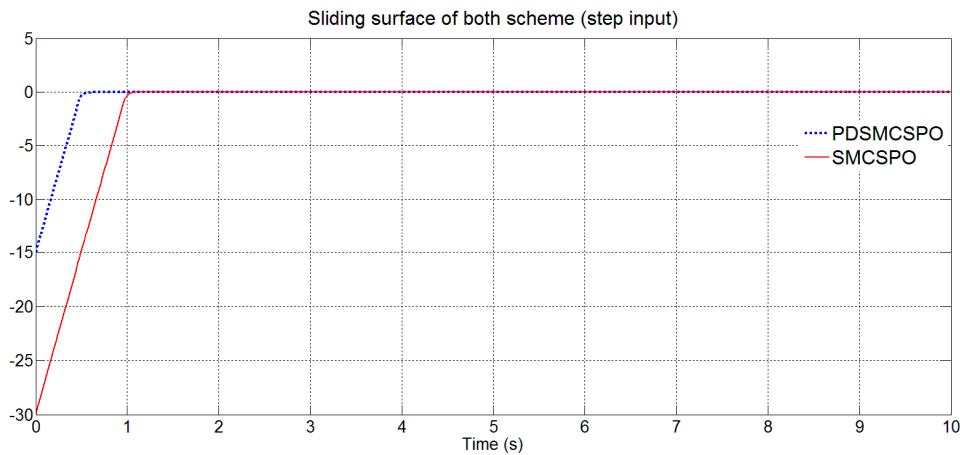


Figure 13. Sliding surface response of both schemes.

To understand the mathematics of control theory, a sine wave of 1 (rad/s) with an amplitude of 1 was given to the system with $\lambda = 30$ and a disturbance which was the sum of a constant (100), a sine and cosine wave of different frequencies were given to the system, and the following results were observed.

3.2.5. Output Error over Perturbation

As it has been discussed in Chapter 2 that our proposed scheme for PDSMCSP0 has more attenuation capability compared to SMCSPO. In Figure 14, it is visible that the trajectory tracking error in the case of SMCSPO is larger than our proposed scheme. The dotted blue line is the error trajectory of PDSMCSP0 and the solid red line about SMCSPO.

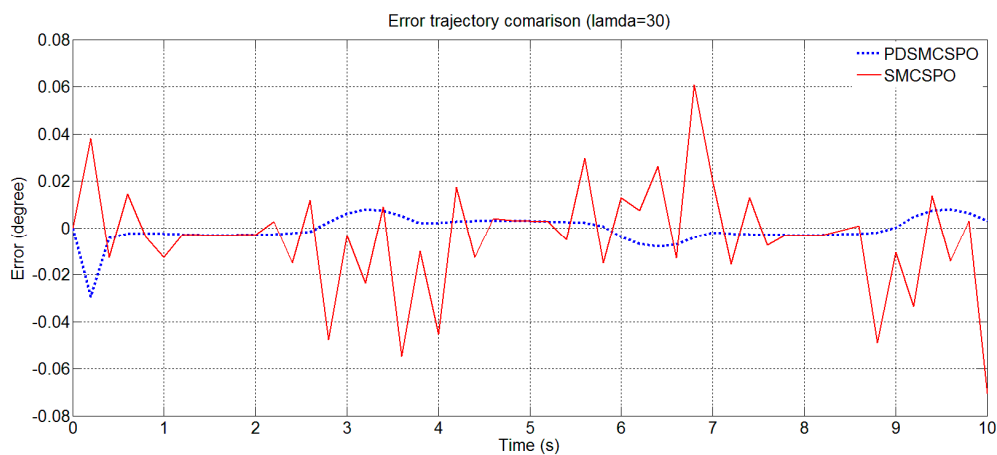


Figure 14. Error trajectory comparisons of both schemes.

3.2.6. Sliding Surface over Perturbation

As was mentioned in Chapter 2, the effect of the perturbation signal on the sliding surface in our proposed scheme was less than conventional SMCSPO. In Figure 2, it can be seen that PDSMCSP0 attenuated the perturbation signal more than SMCSPO, which can be noticed in Figure 15. The solid red line is the sliding surface of SMCSPO, which was affected more by perturbation compared to the dotted blue line for PDSMCSP0.

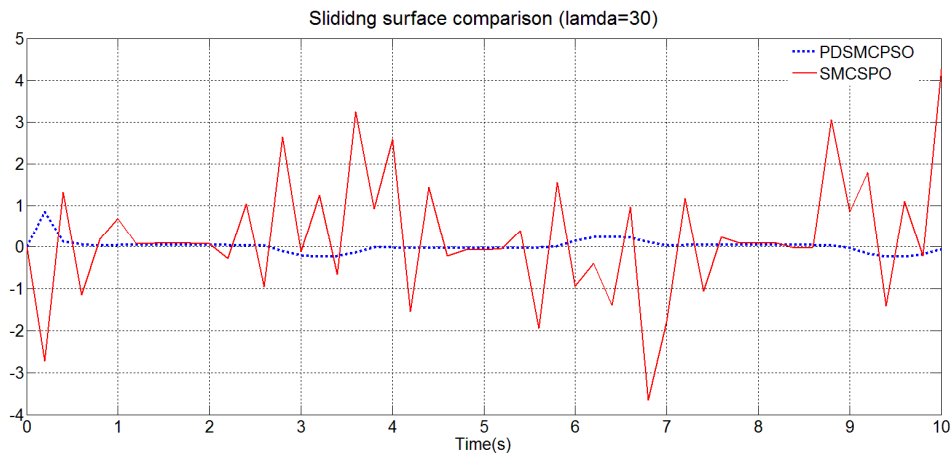


Figure 15. Sliding surface over perturbation of both schemes.

3.3. Experimental Results

For the experiment, the third link of the hydraulic robot manipulator in Figure 4 was considered. It was known that the hydraulic system was highly non-linear in nature and had many uncertainties. As a result, the controller without an observer like SMC and PDSMC, did not have a good performance. Therefore, only two controllers with perturbation compensation have been implemented on the real system. An input sine wave was given to the real system, and the experiment was done with different values of lambda (20 and 30). The desired trajectory was a sine wave with a frequency of 1 (rad/s).

The experimental result of the error trajectory between SMCSPO and PDSMCPSO is shown in Figure 16 with lambda = 20. The parameters of both algorithms are the same as those used in the simulation. The solid red line shows the error trajectory of SMCSPO. As we can see, SMCSPO had more error than PDSMCPSO. The reason was that PDSMCPSO had more attenuation towards the perturbation signal during the sliding phase as discussed before (Figure 14). The dotted blue line is the error trajectory of PDSMCPSO which has a smaller error.

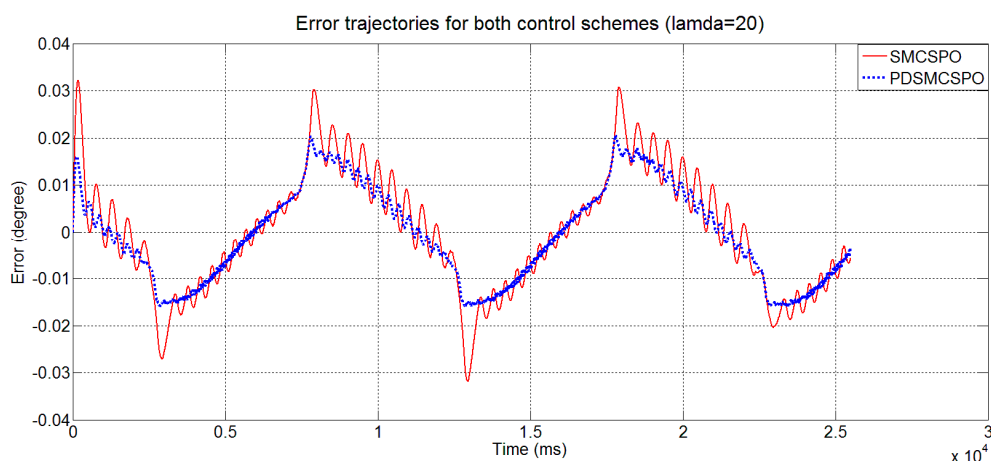


Figure 16. Error trajectories of both control schemes (lambda = 20).

In the next experiment, the value of lambda was increased from 20 to 30. As it is shown in Figure 17, with an increase in the value of lambda, the attenuation of the perturbation signal increases. As a result, error decreases, which can be seen in Figure 17. The solid red line is the error trajectory of SMCSPO, and the blue line is the error trajectory of PDSMCPSO. The trajectory error was reduced in both cases because of the increment in the value of lambda.

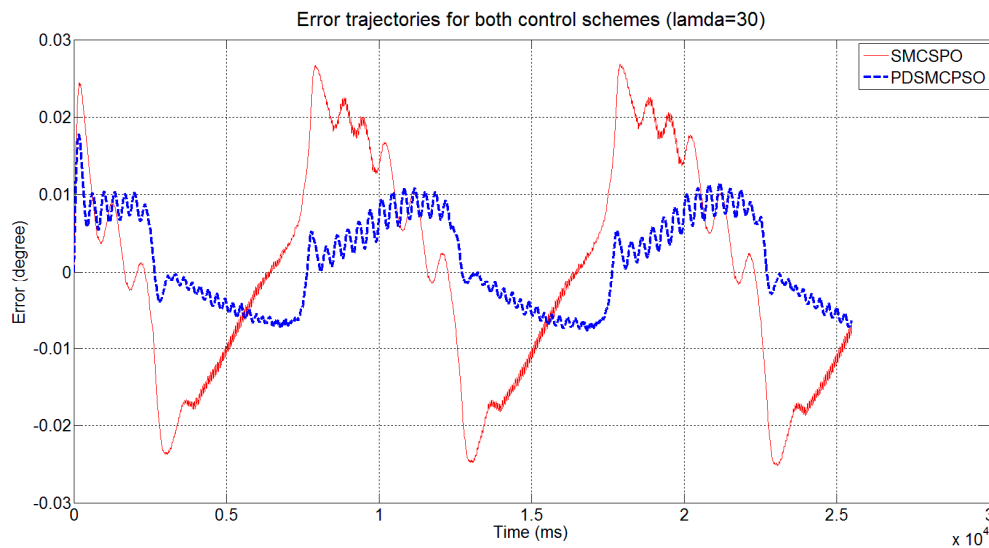


Figure 17. Error trajectories of both control schemes ($\lambda = 20$).

4. Conclusions

In this research, a new robust control algorithm was proposed by altering the sliding surface of conventional SMC. The control performance of SMC, PDSMC, SMCSPO, and PDSMCSPO were compared through simulation and experimental results. The multiplication of small gain k_d with the velocity error term in the sliding surface reduced chattering from the system output as well as the sliding surface. During the sliding phase, this small gain was less than unity, which is multiplied with the perturbation and reduced the effect of perturbation on the system. As a result, a smaller value of switching gain was required compared to conventional SMC. The smaller the value of switching gains, the smaller the chattering. This small gain k_d had shrunk the pass band of the low pass filter between the sliding surfaces over perturbation. Because of that, during the sliding phase, the system remained insensitive to high-frequency perturbation.

The integration of PDSMC in SPO generated a more robust control scheme that used a perturbation compensation technique. It was observed that the convergence of output to the desired states was faster in PDSMCSPO compared with conventional SMCSPO. In this new scheme, the effect of estimation error of state on the estimated sliding surface was reduced. During the sliding phase, the system remained insensitive from perturbation because the Bode plot between error and perturbation had more attenuation capability compared with conventional SMCSPO. The bode plot between the sliding surface and perturbation also has more attenuation capacity compared with previous techniques. This new robust control scheme shows outstanding performance which includes faster convergence to the desired state and less error in both output and sliding surface when compared with SMCSPO in both simulation and experimental results.

Author Contributions: Conceptualization, S.J.A. and M.C.L.; Formal analysis, S.J.A., K.D.K.; Funding acquisition, M.C.L.; Methodology, S.J.A.; Software S.J.A., K.D.K.; Supervision, M.C.L.; Writing-original draft, S.J.A.; Writing-review & editing, S.J.A., K.D.K.

Funding: This research was funded and conducted under the Competency Development Program for Industry Specialists of the Korean Ministry of Trade, Industry and Energy (MOTIE), operated by Korea Institute for Advancement of Technology (KIAT). (The development of high skilled and innovative manpower to lead the Innovation based on Robot).

Acknowledgments: This research was supported by the MOTIE (Ministry of Trade, Industry & Energy), Korea, under the Industry Convergence Liaison Robotics Creative Graduates Education Program supervised by the KIAT (N0001126). This research was supported by the Technology Innovation Program(10073147, Development of Robot Manipulation Technology by Using Artificial Intelligence) funded by the Ministry of Trade, Industry, and Energy(MOTIE, Korea).

Conflicts of Interest: The authors declare no conflict of interest.

References

1. Reuters, Global News, Adivision of Corus Entertainment Inc. Available online: <https://globalnews.ca/news/3286191/robots-to-play-key-role-in-dismantling-nuclear-reactors-at-fukushima> (accessed on 14 November 2018).
2. Jie, W.; Kallu, K.D.; Kim, H.H.; Lee, M.C. TSMCSPO based position control for a hydraulic manipulator. In Proceedings of the 18th International Conference on Control, Automation and Systems (ICCAS), Yong Pyong Resort, Pyeong Chang, Korea, 17–20 October 2018.
3. Truong, D.Q.; Truong, B.N.M.; Trung, N.T.; Nahian, S.A.; Ahn, K.K. Force reflecting joystick control for applications to bilateral teleoperation in construction machinery. *Int. J. Precis. Eng. Manuf.* **2017**, *18*, 301–315. [[CrossRef](#)]
4. Peñaloza-Mejía, O.; Márquez-Martínez, L.A.; Alvarez-Gallegos, J.; Alvarez, J. Master-slave teleoperation of under actuated mechanical systems with communication delays. *Int. J. Control Autom. Syst.* **2017**, *15*, 827–836. [[CrossRef](#)]
5. Mellah, R.; Guermah, S.; Toumi, R. Adaptive control of bilateral teleoperation system with compensatory neural-fuzzy controllers. *Int. J. Control Autom. Syst.* **2017**, *15*, 1949–1959. [[CrossRef](#)]
6. Farooq, U.; Gu, J.; El-Hawary, M.; Asad, M.U.; Abbas, G. Fuzzy model based bilateral control design of nonlinear tele-operation system using method of state convergence. *IEEE Access* **2016**, *4*, 4119–4135. [[CrossRef](#)]
7. Kallu, K.D.; Abbasi, S.J.; Yaqub, M.A.; Lee, M.C. Tele-operated bilateral control of hydraulic servo system using estimated reaction for ceofen deffector by SMCSPPO. In Proceedings of the 15th International Conference on Ubiquitous Robots and Ambient Intelligence (URAI), Honolulu, HI, USA, 26–30 June 2018.
8. Lawrence, D.A. Stability and transparency in bilateral teleoperation. *IEEE Trans. Robot. Autom.* **1993**, *9*, 624–637. [[CrossRef](#)]
9. Terra, M.J.; Elmali, H.; Olgac, N. Sliding Mode Control with Sliding Perturbation Observer. *J. Dyn. Syst. Meas. Control* **1997**, *119*, 657–665.
10. Elmali, H.; Olgac, N. Sliding mode control with perturbation estimation (SMCPE): A new approach. *Int. J. Control* **1992**, *56*, 923–941. [[CrossRef](#)]
11. Slotine, J.J.; Sastry, S.S. Tracking control of nonlinear system using sliding surfaces with application to robot manipulators. *Int. J. Control* **1983**, *38*, 465–492. [[CrossRef](#)]
12. Butt, Q.; Bhatti, A.I. Estimation of gasoline-engine parameters using high order sliding mode control. *IEEE Trans Ind. Electron.* **2008**, *55*, 3908–3916. [[CrossRef](#)]
13. Young, K.D.; Ozguner, U. Sliding Mode: Control Engineering in practice. In Proceeding of the American Control Conference, San Diego, CA, USA, 2–4 June 1999.
14. Yan, X.G.; Spurgeon, S.K.; Edwards, C. Introduction. In *Variable Structure Control of Complex Systems. Communications and Control Engineering*; Springer: Cham, Switzerland, 2017.
15. Abbasi, S.J.; Kallu, K.D.; Jie, W.; Lee, M.C. Robust control design for 2 link robotic manipulator. In Proceedings of the 13th Korea Robotics Society (KRoC), Gangwon, Korea, 21–24 January 2018.
16. Abbasi, S.J.; Kallu, K.D.; Lee, M.C. Comparison of robustness of SMC and PD control of 2 link robot manipulator. In Proceedings of the AROB, Busan, Korea, 5–6 September 2017.
17. Liu, X.; Jiang, W.; Dong, X.C. Nonlinear adaptive control for dynamic and dead zone uncertainties in robotic systems. *Int. J. Control Autom. Syst.* **2017**, *15*, 875–882. [[CrossRef](#)]
18. Li, S.; Yang, J.; Chen, W.H.; Chen, X. Genralized Extended State Observer Based Control for System with Mismatched Uncertainties. *IEEE Trans. Ind. Delect.* **2012**, *59*, 4792–4802. [[CrossRef](#)]
19. Guo, B.Z.; Zhao, Z.L. *Extended State Observe for Nonlinear System with Uncertainty*; IFAC: Milano, Italy, 2011.
20. Jie, W.; Kallu, K.D.; Lee, M.C. A reaction force estimation method of end effector of two link manipulator using SMCSPPO. In Proceedings of the 13th International Conference on Ubiquitous Robots and Ambient Intelligence (URAI), Xian, China, 19–22 August 2016.
21. Kallu, K.D.; Jie, W.; Lee, M.C. PDSPO based estimation of reaction force of end effector of two link manipulator without sensor. In Proceedings of the Society of Instrument and Control Engineers (SICE), Tsukuba, Japan, 2023 September 2016.
22. Kallu, K.D.; Jie, W.; Lee, M.C. Sensorless reaction force estimation of the end effector of a dual-arm robot manipulator using Sliding Mode Control with Sliding Perturbation Observer. *Int. J. Control Autom. Syst.* **2018**, *16*, 1367–1378. [[CrossRef](#)]

23. Kallu, K.; Wang, J.; Abbasi, S.; Lee, M. Estimated reaction force based bilateral control between 3DOF master and hydraulic slave manipulators for dismantlement. *Electronics* **2018**, *7*, 256. [[CrossRef](#)]
24. Abbasi, S.J.; Kallu, K.D.; Lee, M.C. Efficient control of non-linear system using modified sliding mode control. In Proceedings of the Society of Instrument and Control Engineers (SICE), Nara, Japan, 11–14 September 2018.
25. Lee, M.C.; Aoshima, N. Identification and its evaluation of the system with an on linear element by signal compression method. *Trans. Soc. Instrum. Control Eng.* **1989**, *25*, 729–736. [[CrossRef](#)]



© 2019 by the authors. Licensee MDPI, Basel, Switzerland. This article is an open access article distributed under the terms and conditions of the Creative Commons Attribution (CC BY) license (<http://creativecommons.org/licenses/by/4.0/>).